

**Production and Thermal Equilibration of Partons
in
Relativistic Heavy Ion Collisions:
 $\sqrt{s} = 20$ vs. 200 A·GeV**

Dinesh Kumar Srivastava

*Variable Energy Cyclotron Centre,
1/AF Bidhan Nagar, Calcutta 700 064, India
and*

*Fakultät für Physik, Universität Bielefeld, D-33501, Bielefeld,
Germany*

Abstract

The production and thermalization of partons liberated in relativistic heavy ion collisions is investigated within the parton cascade model. The momentum distribution of the partons near $z = 0$ is found to become isotropic beyond about 1 fm/ c after the overlap for the collision of lead nuclei at $\sqrt{s} = 20$ A·GeV indicating a thermalization. At $\sqrt{s} = 200$ A·GeV this is attained by about 0.5 fm/ c after the complete overlap.

1 Introduction

The search for quark-gluon plasma, the deconfined strongly interacting matter, has entered a decisive phase with the relativistic heavy ion collision experiments slated to begin within a few months at the Brookhaven National Laboratory. This will put the scores of theoretical models, conjectures, and speculations put forward over the last decade as plausible signatures of quark gluon plasma (QGP) [1] to a severe test. The corresponding search at the CERN SPS has already yielded a large body of data which have been carefully examined for the evidence of QGP. It has been suggested that it is quite likely that the partonic phase may, indeed, have been reached in sulfur and lead induced collisions at the CERN SPS [2].

The parton cascade model proposed by Geiger and Müller [3] and refined and studied exhaustively by Geiger and coworkers [4] attempts to describe the relativistic collision of nuclei using the partonic picture of hadronic interactions where the nuclear dynamics is described in terms of quark and gluon interactions within perturbative QCD, embedded in the frame work of relativistic transport theory. The complete space-time picture of the evolution is simulated by solving an appropriate transport equation in six-dimensional phase space using Monte Carlo techniques. The model supplemented with a cluster hadronization scheme has been developed into a computer code VNI [5]. It was recently shown to give a reasonable description to particle spectra at SPS energies for $S + S$ and $Pb + Pb$ collisions [6], which needs to be understood in a greater detail in view of the suggestion made in Ref. [2].

In the present work we continue this effort [7] and use the power of the parton cascade model to see how quickly does the partonic matter produced in such collisions thermalize at CERN SPS and BNL RHIC energies. It should be added that this question has been studied within the context of RHIC (and LHC) energies by Geiger [4], and we display them somewhat differently (and with much better statistics) for a ready and easy comparison.

Even though the developments in the parton cascade model have been very well documented, it is worthwhile recalling the most important steps:

- The *initial state* associated with the incoming nuclei involves their decomposition into nucleons and of the nucleons into partons on the basis of experimentally measured nucleon structure functions and elastic form factors. This procedure then translates the initial nucleus-nucleus system into two colliding clouds of virtual partons.
- The *parton cascade development* starts from the initial inter-penetrating parton clouds and traces their space-time development with mutual interactions and self interactions of the system of quarks and gluons. The model includes *multiple* elastic and inelastic interactions described as sequences of elementary $2 \rightarrow 2$ scatterings, $1 \rightarrow 2$ emissions, and $2 \rightarrow 1$ fusions. Several important effects which characterize the space-time evolution of a many parton system in nuclear collisions like the individual time scale of each parton-parton collision, the formation time of the parton radiation, the effective suppression of radiative emissions from virtual partons due to an enhanced absorption probability of others in regions of dense phase space occupation, and the effects of soft gluon interference in low energy gluon emissions are explicitly accounted for.
- And finally, the *hadronization dynamics* of the evolving system in terms of a par-

ton coalescence to colour neutral clusters is described as a local statistical process that depends on the spatial separation and colour of the nearest-neighbour partons [8]. The pre-hadronic clusters then decay to form hadrons.

In the present paper we shall be concerned with only up to the second stage of the collision, for times ≤ 2 fm/ c so that the matter is still in the form of primary, secondary, and space-like partons and which essentially spans the so-called pre-equilibrium era of the evolution.

We consider four cases: $S + S$ and $Pb + Pb$ collisions at $\sqrt{s} = 20$ A·GeV and 200 A·GeV. In all the cases we place the two nuclei centred at $z = \pm 1$ fm at $t = -1$ fm/ c , which will propel them on to a complete overlap at around $t = 0$ fm/ c .

We analyze the results for the time evolution of the longitudinal and rapidity distribution of partons and also see how the thermalization is attained and maintained, if at all.

It should be added right at the outset that only the ‘real’ partons have been included in these spectra [3]. Thus the initial state, before the collision will reflect only the distribution of valence quarks, and as the collision proceeds more and more of the (initially) space-like gluons and sea-quarks gain enough energy to become either time-like or be on the mass-shell. One may also add that the rapidity variable is not defined for space-like particles (as for them $E < |p_z|$) and moreover, the partons which remain space-like throughout the collision do not contribute to the reaction dynamics and will be reabsorbed during the hadronization.

2 $\sqrt{s} = 20$ A·GeV

2.1 Production of (semi)hard partons

In Fig. 1, we have shown the time development of the longitudinal distribution of (real) partons for $S + S$ collision at 20 A·GeV. We see that the the partonic distributions almost touch when $t = -0.4$ fm/ c and the nuclei disengage by $t \approx 1$ fm/ c , leaving a trail of secondary partons near $z = 0$, which are created in the (semi)hard collisions and radiations.

The evolution of the rapidity distribution of the partons for $S + S$ collisions is shown in Fig. 2. We see that initially they are distributed over about four units of rapidity, and peak around $y = \pm 2$. As a result of the collision the number of partons

having $y \approx \pm 2$ gets reduced, and most of the secondary partons materialize by the time $t = 0.4 \text{ fm}/c$. They are seen to be confined to $|y| \leq 2$. Approximating the width of the region over which the secondary partons are spread, as $\Delta y \approx 4$, we see that there is a production of about two partons per participating nucleon. The dip in the rapidity distribution is quite interesting too, as it implies that a large part of the partons have just passed through, without interacting.

The situation for the collision of lead nuclei is quite different. We see (Fig. 3) that the nuclei start touching at $t = -0.8 \text{ fm}/c$ and there is already a considerable overlap by the time $t = -0.4 \text{ fm}/c$. The nuclei disengage only by $t \approx 1.5 \text{ fm}/c$, leaving a trail of secondary partons in their wake.

The differences between the two cases are much more dramatic, when we look at the evolution of the rapidity distribution of the partons (Fig. 4). Thus we see that there is a considerable production of partons already at $t = 0 \text{ fm}/c$, even when the nuclei have not yet ploughed through each other. The particle production continues till about $1.2 \text{ fm}/c$ which is clear from the modification of the rapidity distribution till then. We also see that now the parton production is much more, the dip at $y = 0$ in the rapidity distribution before the collision is completely filled up by the end of the collision, and we have a flat top distribution of partons! We also see that again the secondary partons are spread over $|y| \leq 2$ and up to four partons per participating nucleon are produced. Recalling that the nuclei would be thicker at smaller transverse distances from the collision axis and that nucleons there are more likely to re-scatter, these observations imply a considerable multiple scattering among the partons.

2.2 Thermalization of partons

As indicated in the Introduction, the thermalization of partons has been addressed in detail in the parton cascade model studies. Several phenomenological estimates have also been obtained in the literature [9]. We adopt a slightly different strategy here and look at the $|p_x|$, $|p_y|$, and $|p_z|$ distribution of the materialized partons at different times in the centre of mass system of the colliding nuclei. We confine our attention to $|z| \leq 0.5 \text{ fm}$, and determine whether these distribution become isotropic at some stage during the evolution. A similar approach was used in Ref. [10] when only the radiation of the gluons following the first (semi)hard scatterings was included in such collisions. However, it is expected that multiple scatterings included in the parton cascade model used in the present work will hasten this process and also maintain the thermal equilibrium. In absence of the multiple scatterings a thermal equilibrium can neither be achieved nor maintained.

The results of our simulations for $S + S$ collisions at $\sqrt{s} = 20$ A·GeV are shown in Fig. 5. We see that the scatterings which began even before $t = 0$ fm, (see Figs. 1 & 2) increase the value of $\langle |p_x| \rangle$ and $\langle |p_y| \rangle$ and decreases the $\langle |p_z| \rangle$, as seen from the reduction of the number of partons having large $|p_z|$ and their reappearance with smaller $|p_z|$. There will also be an escape of partons which have a large rapidity from the zone $|z| \leq 0.5$ fm chosen here. As a result of these two processes the momentum distribution becomes isotropic around $t = 1$ fm/ c , and stays so for a brief while after that.

The corresponding results for $Pb + Pb$ collisions (Fig. 6) are similar in nature and we see that the number of partons released is much larger in the heavier system. Isotropy of the momenta is attained in the system near $z = 0$ around $t = 1$ fm/ c which is maintained afterwards.

Thus we conclude that the partonic system produced in heavy-ion collisions at $\sqrt{s} = 20$ A·GeV will have an excursion into a thermalized zone at about 1 fm/ c after the nuclei overlap as a result of (semi)hard partonic collisions and gluonic radiations.

3 $\sqrt{s} = 200$ A·GeV

While the attempt to use the parton cascade model at such low energies as $\sqrt{s} = 20$ A·GeV are rather recent, those at the energies relevant to BNL RHIC, 200 A·GeV, are quite well documented and thus we shall give only the results for the rapidity distribution and the approach to isotropic momenta in the central zone of the collision volume.

3.1 Production of (semi)hard partons

Thus in Fig. 7 we have shown the time evolution of the rapidity distribution of the real partons for central collisions of sulfur nuclei. As before the dashed histograms show the results for the primary (uninteracted) partons while the solid histograms show the sum of the primary and the secondary (semi)hard partons produced in the collision. We note that the production of partons in the parton cascade approach utilized here is completed by 0.4 fm/ c after the nuclei overlap fully. We can also estimate that the up to 6 partons per ‘participating’ nucleon may be produced in these collisions which are spread over $|y| \leq 2.5$.

The corresponding results for central collisions of lead nuclei (Fig. 8) are very re-

vealing, as the dip in the rapidity distribution of the partons is much less pronounced, as a result of a much larger production of partons due to multiple scatterings. We also estimate that up to 9 partons per nucleon may be produced in this case.

Before moving on, it is of interest to note that the shape of the initial state parton distribution here is different from the one in Fig. 2 (at 20 A·GeV) as we prepare the assembly of the partons at a higher Q_0^2 (see, Discussion), resulting in a higher number of partons at the lower end of x , which translates into smaller $|y|$ in this plot.

3.2 Thermalization of partons

The evolution of the momentum distribution of the partons produced due to the (semi)hard scatterings and radiations are shown in Fig. 9 and 10 respectively for the central collisions of sulfur and lead nuclei at energies relevant to BNL RHIC. We see that initially the partons have a large $|p_z|$, (note also the dip at $|p_z| \approx 0$, depicting the separation of the partons in the rapidity space) and the collisions transfer p_z into p_x and p_y which increase substantially and rapidly. The peak in the $|p_z|$ spectrum around 1 GeV holds the primary partons which have not interacted yet. We note that by the time $t = 0.4$ fm/ c the slopes of the momenta along the three direction are similar, but for the above mentioned peak, which persists till the end. Ignoring these uninteracted partons, we see that the partons which materialize during the collision attain an isotropic momentum distribution by $t \approx 0.5$ fm/ c . Once again, the partons having large rapidities will escape the longitudinal slice which we have considered.

4 Discussion

Before concluding it is worthwhile that some aspects of the model used for the studies reported here are reiterated. The first one concerns the so-called p_0 which is used to divide the scatterings in the parton cascade model into soft (elastic) and (semi)hard reactions. It is taken as 1.12 GeV for the collisions at 20 A·GeV and 2.09 GeV for collisions at 200 A·GeV based on considerations of pp cross-sections discussed in detail [3, 4]. There is no reason to believe that they should have the same values for nuclear collisions, but these provide a convenient starting point. An increase in p_0 will obviously decrease the (semi)hard scatterings. The scale Q_0 at which the nucleon structure functions are initialized are chosen as 1.32 and 2.35 GeV at the two energies, based on an estimate of $\langle p_T^2 \rangle$ in primary-primary collisions among the primary partons. We have already remarked that a larger Q_0 leads to the different

shapes for the rapidity distributions at the higher energy considered here.

A careful reader must have noticed that the transverse components of the momenta “stabilize” fairly quickly. This has its origin in the fact that *no* collisions between partons is permitted, if their relative \sqrt{s} is less than 2 GeV. This is done to ensure that the perturbative QCD treatment used in the parton cascade model remains valid. Again, a parton created in a scattering with a large momentum loses energy quickly due to gluonic radiations (till its virtuality drops to the cut-off $\mu_0 \approx 1$ GeV chosen in the calculations) and its momentum is considerably reduced before it undergoes next collision. When the initial energy is high and the parton density is large, it may participate in further hard scatterings with production of additional partons, else- it will undergo only soft scatterings (see, e.g., Ref. [7, 11]).

A more comprehensive [12] approach could proceed as follows: use the (practical) procedure of soft and (semi)hard scatterings of the parton cascade model to initiate the collision and once the partonic density is large enough to ensure screening of the long range forces on a scale where the Debye mass μ_D is much larger than Λ_{QCD} , remove the division of soft and hard scatterings implemented in the model; evaluating the scattering in terms of the Debye mass at *all* possible \sqrt{s} between partons and for *all* momentum transfers. This treatment will, however, quickly get beyond the capability of most of the computers due to the very large number of scatterings taking place. The other and more serious problem will involve the comparatively small number of partons in a given event to implement this scheme over the entire space-time spanned by the system as then we would be plagued by large fluctuations. A more practical approach [13] could be to invoke hydrodynamics to pursue the evolution [14] beyond the point of thermalization, after an average is taken over a large number of events. This is in progress.

5 Conclusions

To conclude, we have seen that the parton cascade model suggests that there is a substantial production of partonic matter as a result of (semi)hard scatterings and QCD branchings in $S + S$ and $Pb + Pb$ collisions at 20 A·GeV, which may attain an isotropy in momentum distribution at about 1 fm/ c after the nuclei overlap completely at $|z| \approx 0$. The simulations reveal an increased multiple scattering activity in lead induced collisions.

The corresponding production at 200 A·GeV is (obviously) much larger and the isotropy in the momentum distribution is attained within 0.5 fm/ c . It is also suggested

that this could be a convenient point to initialize a hydrodynamic approach to the evolution, if desired.

Acknowledgments

The author gratefully acknowledges the hospitality of University of Bielefeld where part of this work was done. He would also like to acknowledge useful comments from Hans Gutbrod and Bikash Sinha.

References

- [1] Physics and Astrophysics of Quark-Gluon Plasma, Ed. B. C. Sinha, D. K. Srivastava, and Y. P. Viyogi, Narosa Publishing House, New Delhi, 1998.
- [2] R. Stock, eprint hep-ph/9901415.
- [3] K. Geiger and B. Müller, Nucl. Phys. B **369**, 600 (1992).
- [4] K. Geiger, Phys. Rep. **258**, 376 (1995) and references there-in.
- [5] K. Geiger, Comp. Phys. Comm. **104**, 70 (1997); K. Geiger, R. Longacre , and D. K. Srivastava; nucl-th/9806102, The results reported here have been obtained using the version 4.09, with the removal of the incorrect rescaling of the space-time co-ordinates. This (incorrect) rescaling was introduced during the transition of the version 4.08 to 4.09. We are grateful to S. Bass for drawing our attention to this.
- [6] K. Geiger and D. K. Srivastava, Phys. Rev. C **56**, 2718 (1997); D. K. Srivastava and K. Geiger, Phys. Lett. B **422**, 39 (1998); K. Geiger, Nucl. Phys. A **638**, 551c (1998); K. Geiger and B. Müller, Heavy Ion Physics **7**, 207 (1998); D. K. Srivastava and K. Geiger, nucl-th/9808042.
- [7] D. K. Srivastava and K. Geiger, Nucl. Phys. A **647**, 136 (1999); D. K. Srivastava and K. Geiger, Phys. Rev. C **58**,1734 (1998); D. K. Srivastava, nucl-th/9901043.
- [8] J. Ellis and K. Geiger, Phys. Rev. D **52**, 1500 (1995); J. Ellis and K. Geiger, Phys. Rev. D **54**, 1967 (1996).

- [9] R. C. Hwa and K. Kajantie, Phys. Rev. Lett. **56**, 637 (1986); J.-P. Blaizot and A. H. Mueller, Nucl. Phys. B **289**, 847 (1987); E. Shuryak, Phys. Rev. Lett. **68**, 3270 (1992); T. S. Biro, E. van Doorn, B. Müller, M. H. Thoma, and X.-N. Wang, Phys. Rev. C **48**, 1275 (1993).
- [10] K. J. Eskola and X.-N. Wang, Phys. Rev. D **49**, 1284 (1994).
- [11] M. Gyulassy and P. Levai, Phys. Lett. B **442**,1 (1998).
- [12] B. Müller, nucl-th/9902065.
- [13] K. J. Eskola, B. Müller, and X.-N. Wang, Phys. Lett. B **374**, 20 (1996).
- [14] D. K. Srivastava, M. G. Mustafa, and B. Müller, Phys. Lett. B **396**, 45 (1997);
D. K. Srivastava, M. G. Mustafa, and B. Müller, Phys. Rev. C **56**, 1064 (1997).

FIGURE CAPTIONS

Fig. 1 Longitudinal distribution of (real) partons in central collision of sulfur nuclei at $\sqrt{s} = 20$ A·GeV, at different times before and after the collision. The solid histograms give the sum of primary and (semi)hard secondary partons, while the dashed histograms give the result for the primary (uninteracted) partons.

Fig. 2 Rapidity distribution of (real) partons in central collision of sulfur nuclei at $\sqrt{s} = 20$ A·GeV, at different times before and after the collision. The solid histograms give the sum of primary and (semi)hard secondary partons, while the dashed histograms give the result for the primary (uninteracted) partons.

Fig. 3 Longitudinal distribution of (real) partons in central collision of lead nuclei at $\sqrt{s} = 20$ A·GeV, at different times before and after the collision. The solid histograms give the sum of primary and (semi)hard secondary partons, while the dashed histograms give the result for the primary (uninteracted) partons.

Fig. 4 Rapidity distribution of (real) partons in central collision of lead nuclei at $\sqrt{s} = 20$ A·GeV, at different times before and after the collision. The solid histograms give the sum of primary and (semi)hard secondary partons, while the dashed histograms give the result for the primary (uninteracted) partons.

Fig. 5 Time evolution of the $|p_x|$ (crosses), $|p_y|$ (diamonds) and $|p_z|$ (histogram) distribution of the (real) partons in central collision of sulfur nuclei at $\sqrt{s} = 20$ A·GeV.

Fig. 6 Time evolution of the $|p_x|$ (crosses), $|p_y|$ (diamonds) and $|p_z|$ (histogram) distribution of the (real) partons in central collision of lead nuclei at $\sqrt{s} = 20$ A·GeV.

Fig. 7 Rapidity distribution of (real) partons in central collision of sulfur nuclei at $\sqrt{s} = 200$ A·GeV, at different times before and after the collision. The solid histograms give the sum of primary and (semi)hard secondary partons, while the dashed histograms give the result for the primary (uninteracted) partons.

Fig. 8 Rapidity distribution of (real) partons in central collision of lead nuclei at $\sqrt{s} = 200$ A·GeV, at different times before and after the collision. The solid histograms give the sum of primary and (semi)hard secondary partons, while the dashed histograms give the result for the primary (uninteracted) partons.

Fig. 9 Time evolution of the $|p_x|$ (crosses), $|p_y|$ (diamonds) and $|p_z|$ (histogram) distribution of the (real) partons in central collision of sulfur nuclei at $\sqrt{s} = 200$ A·GeV.

Fig. 10 Time evolution of the $|p_x|$ (crosses), $|p_y|$ (diamonds) and $|p_z|$ (histogram) distribution of the (real) partons in central collision of lead nuclei at $\sqrt{s} = 200$ A·GeV.

S+S @ 20 AGeV

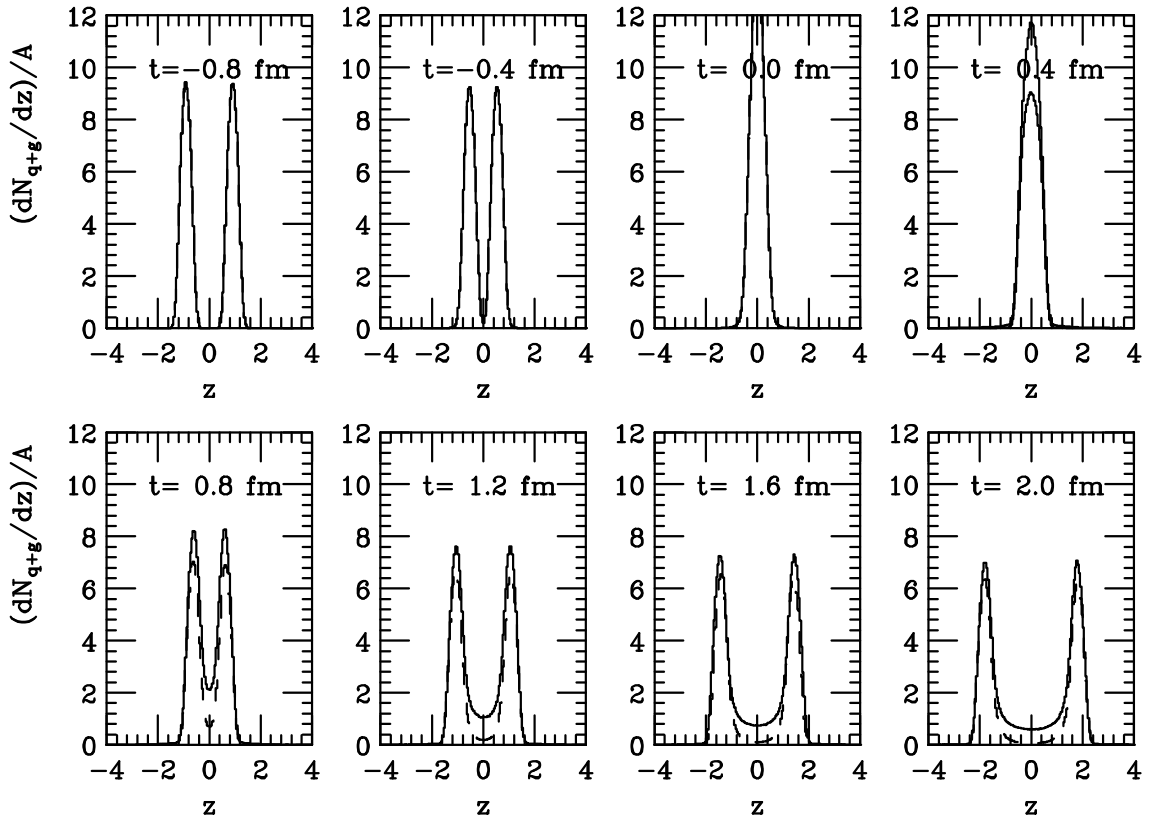


Figure 1: Longitudinal distribution of (real) partons in central collision of sulfur nuclei at $\sqrt{s} = 20$ A·GeV, at different times before and after the collision. The solid histograms give the sum of primary and (semi)hard secondary partons, while the dashed histograms give the result for the primary (uninteracted) partons.

S+S @ 20A GeV

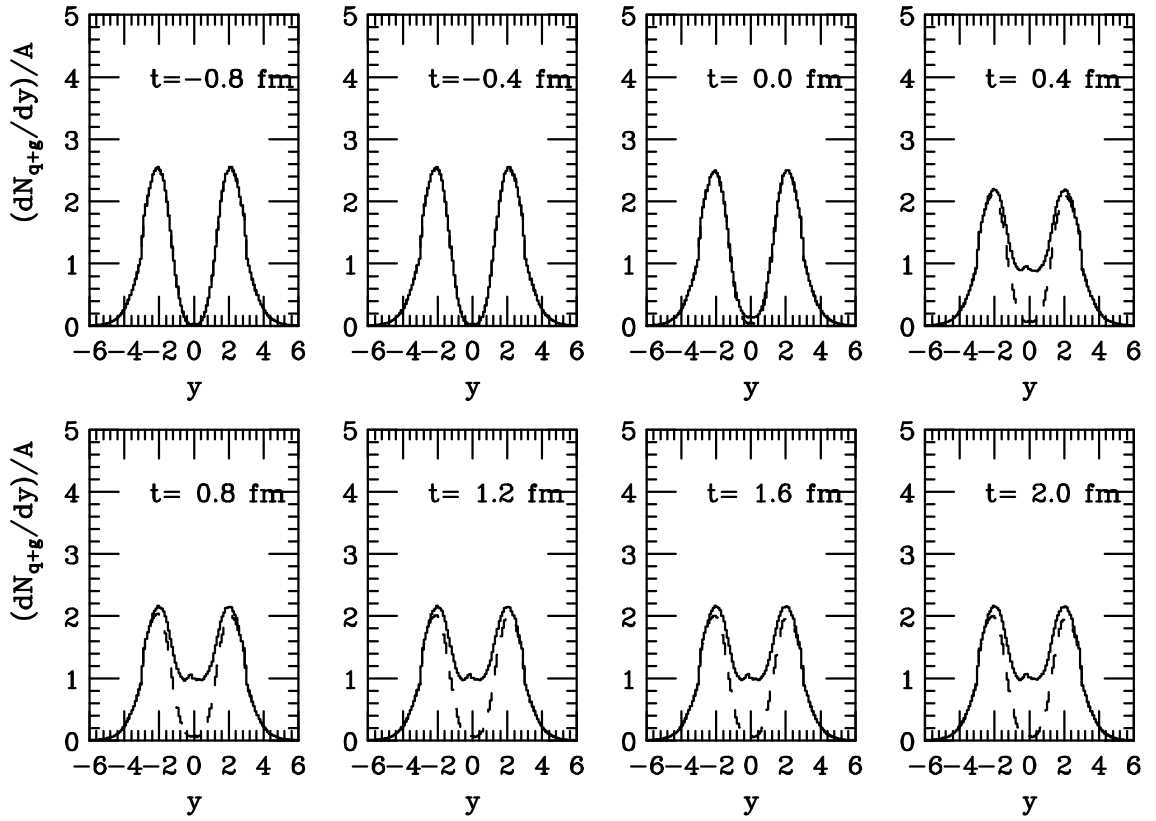


Figure 2: Rapidity distribution of (real) partons in central collision of sulfur nuclei at $\sqrt{s} = 20$ A·GeV, at different times before and after the collision. The solid histograms give the sum of primary and (semi)hard secondary partons, while the dashed histograms give the result for the primary (uninteracted) partons.

Pb+Pb @ 20 AGeV

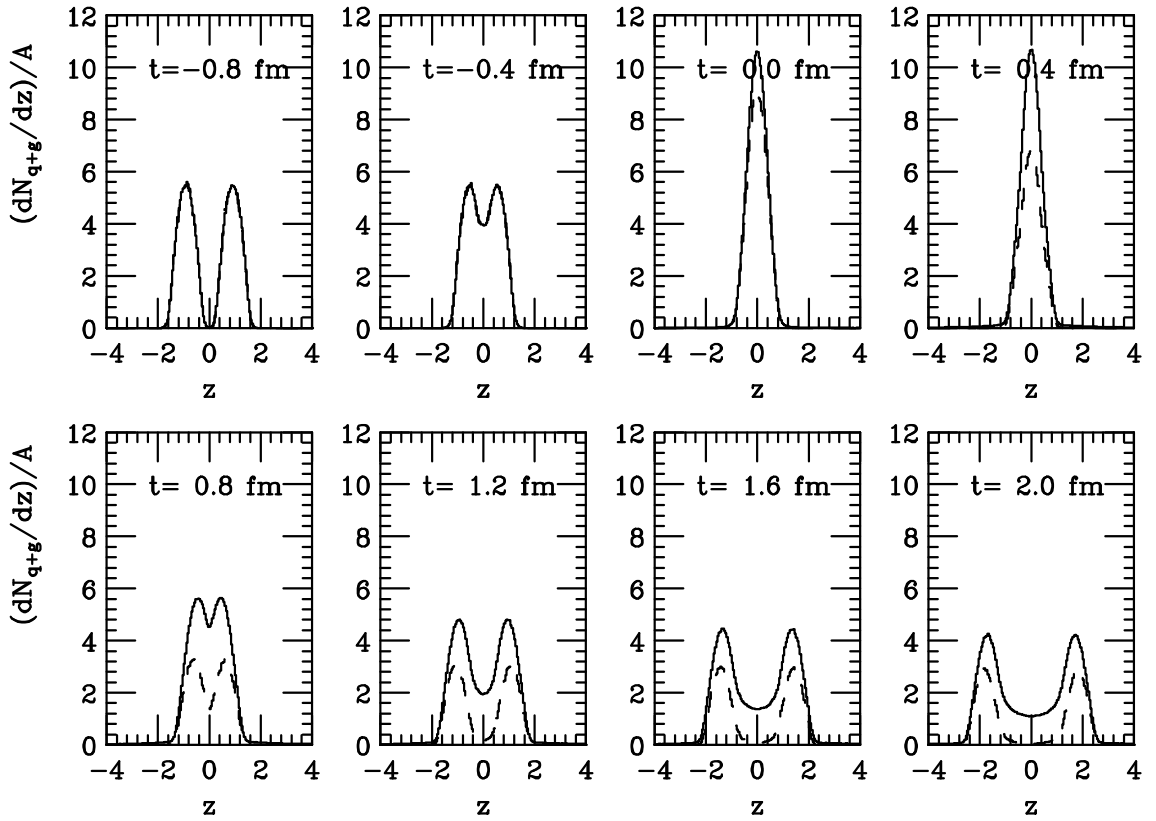


Figure 3: Longitudinal distribution of (real) partons in central collision of lead nuclei at $\sqrt{s} = 20$ A·GeV, at different times before and after the collision. The solid histograms give the sum of primary and (semi)hard secondary partons, while the dashed histograms give the result for the primary (uninteracted) partons.

Pb+Pb @ 20A GeV

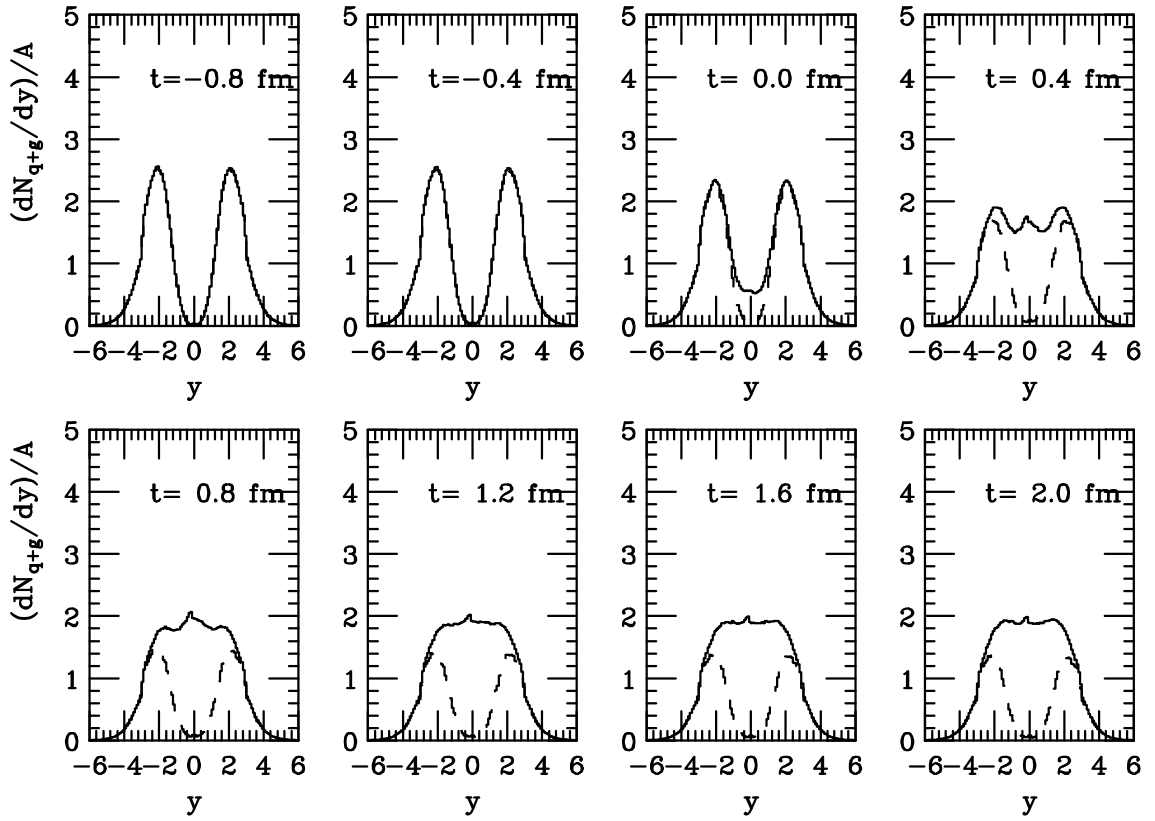


Figure 4: Rapidity distribution of (real) partons in central collision of lead nuclei at $\sqrt{s} = 20$ A·GeV, at different times before and after the collision. The solid histograms give the sum of primary and (semi)hard secondary partons, while the dashed histograms give the result for the primary (uninteracted) partons.

S+S@20 AGeV; $|z| < 0.50$ fm

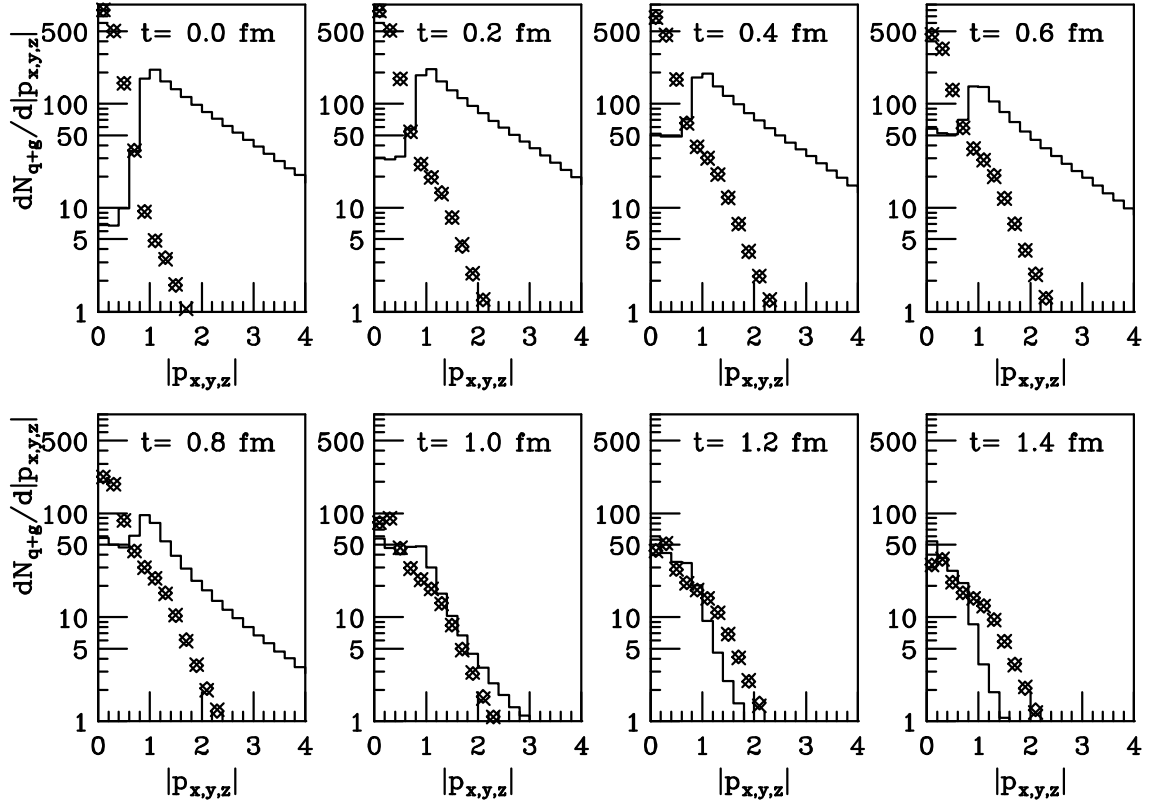


Figure 5: Time evolution of the $|p_x|$ (crosses), $|p_y|$ (diamonds) and $|p_z|$ (histogram) distribution of the (real) partons in central collision of sulfur nuclei at $\sqrt{s} = 20$ A·GeV.

Pb+Pb@20 AGeV; $|z| < 0.50$ fm

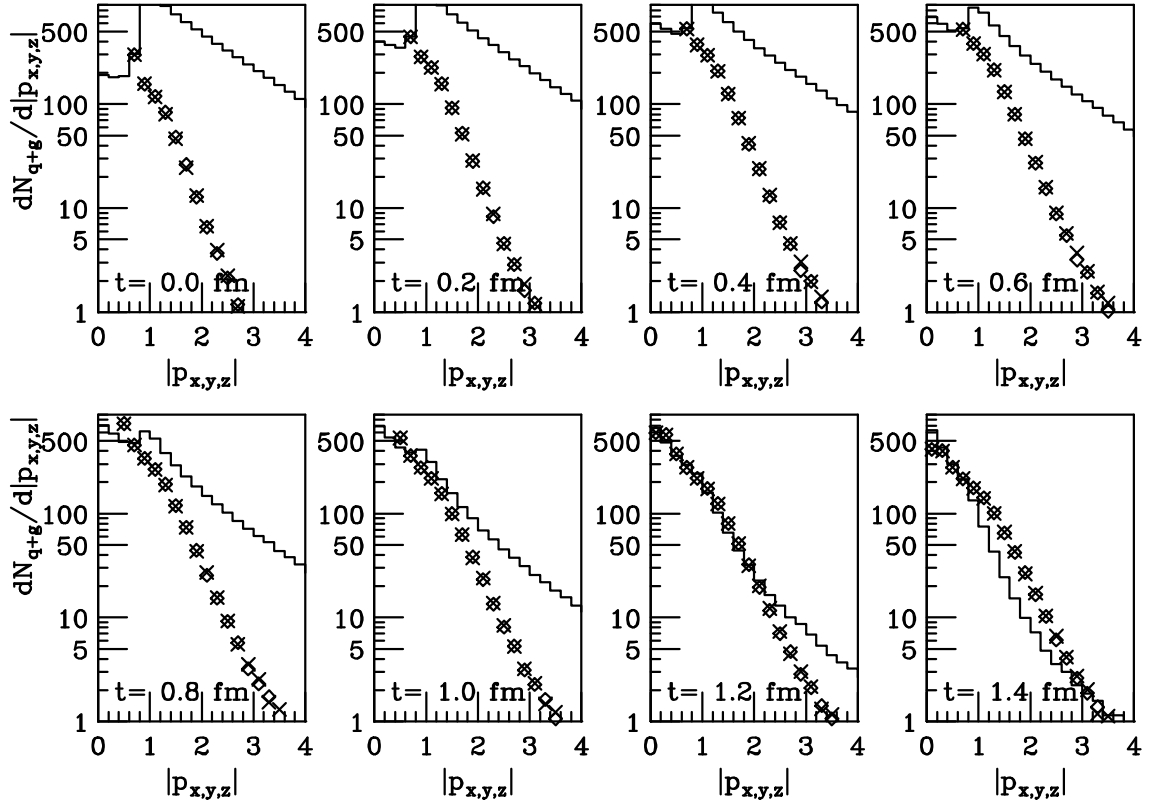


Figure 6: Time evolution of the $|p_x|$ (crosses), $|p_y|$ (diamonds) and $|p_z|$ (histogram) distribution of the (real) partons in central collision of lead nuclei at $\sqrt{s} = 20$ A-GeV.

S+S@ 200 AGeV

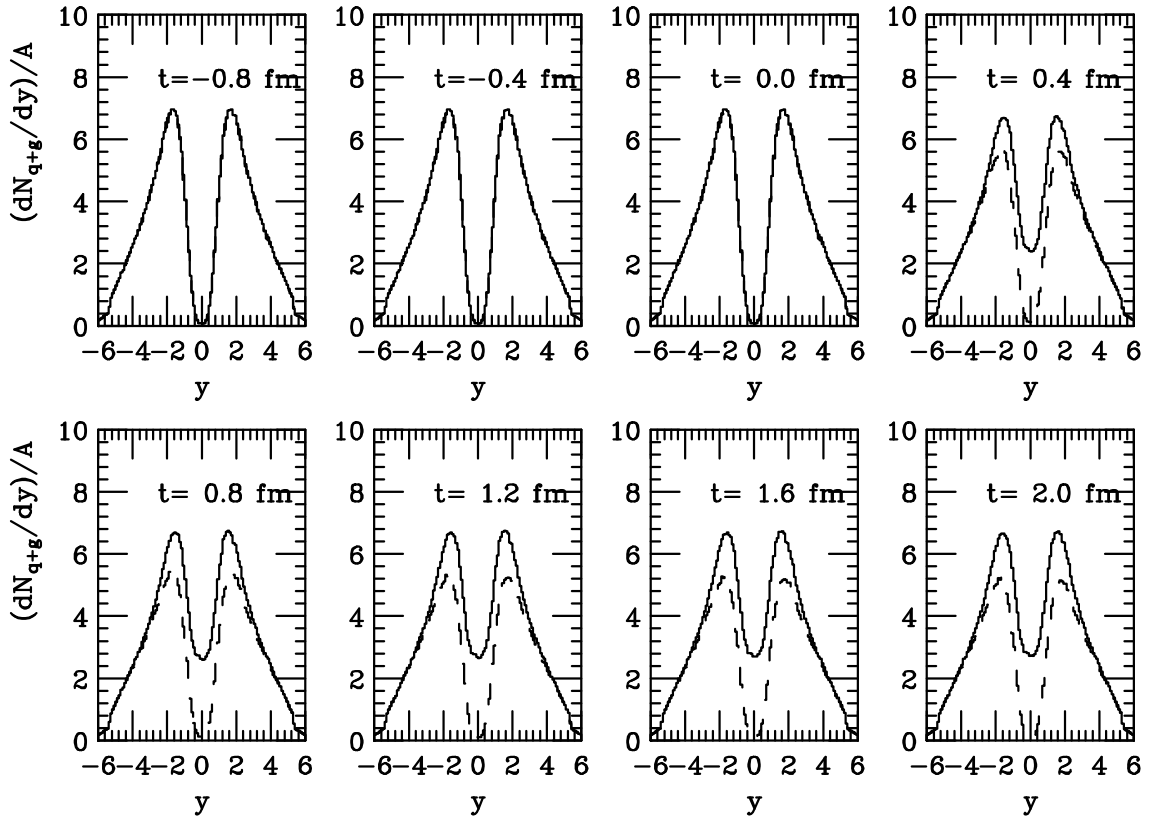


Figure 7: Rapidity distribution of (real) partons in central collision of sulfur nuclei at $\sqrt{s} = 200$ A·GeV, at different times before and after the collision. The solid histograms give the sum of primary and (semi)hard secondary partons, while the dashed histograms give the result for the primary (uninteracted) partons.

Pb+Pb @ 200 AGeV

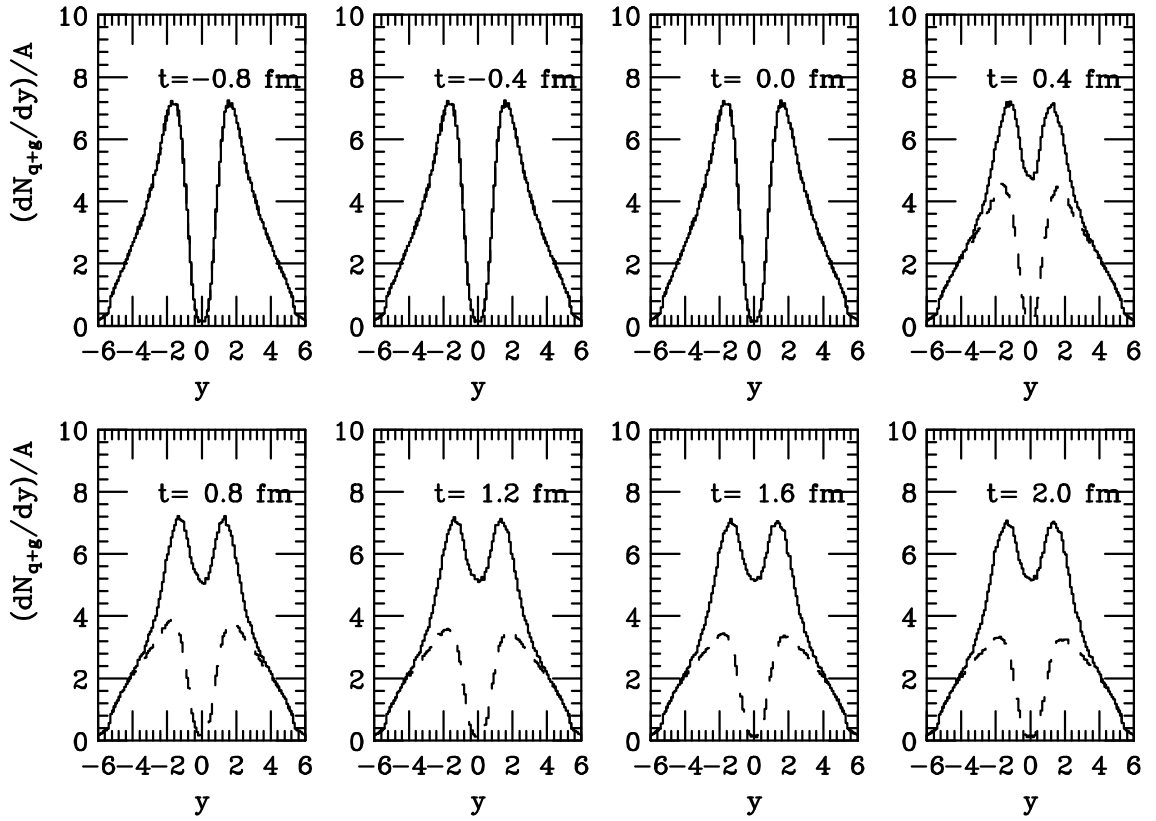


Figure 8: Rapidity distribution of (real) partons in central collision of lead nuclei at $\sqrt{s} = 200$ A·GeV, at different times before and after the collision. The solid histograms give the sum of primary and (semi)hard secondary partons, while the dashed histograms give the result for the primary (uninteracted) partons.

S+S@200 AGeV; $|z| < 0.25$ fm

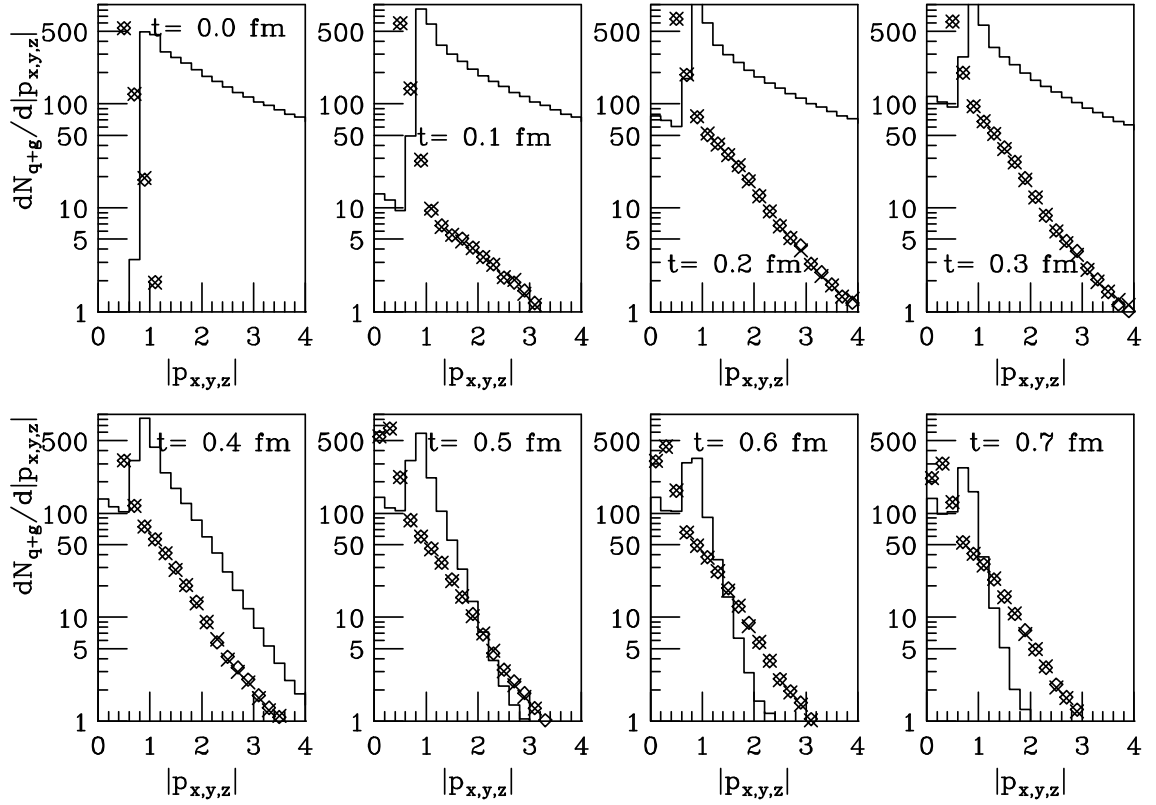


Figure 9: Time evolution of the $|p_x|$ (crosses), $|p_y|$ (diamonds) and $|p_z|$ (histogram) distribution of the (real) partons in central collision of sulfur nuclei at $\sqrt{s} = 200$ A·GeV.

Pb+Pb @ 200A GeV; $|z| < 0.25$ fm

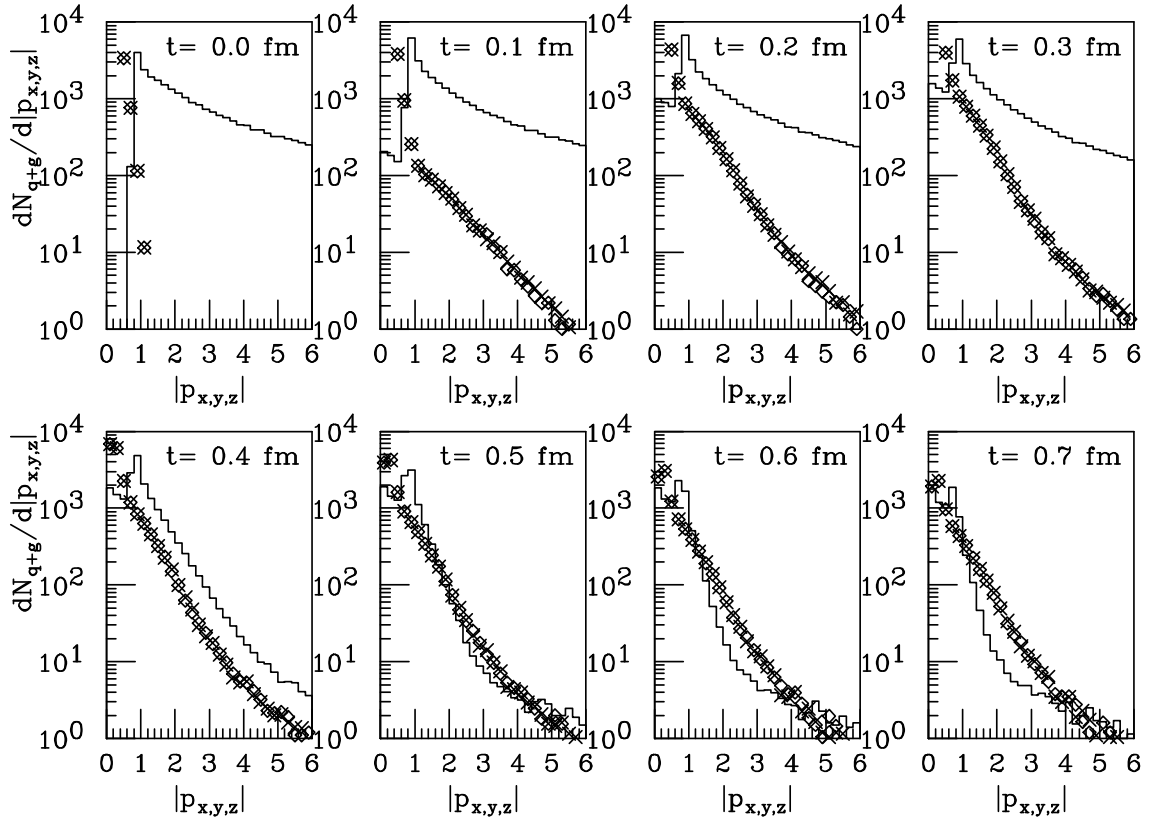


Figure 10: Time evolution of the $|p_x|$ (crosses), $|p_y|$ (diamonds) and $|p_z|$ (histogram) distribution of the (real) partons in central collision of lead nuclei at $\sqrt{s} = 200$ A·GeV.